Structure, Magnetic Behavior, and Anisotropy of Homoleptic Trinuclear Lanthanoid 8-Quinolinolate Complexes

Nicholas F. Chilton,[†,‡] Glen B. Deacon,[†] Olga Gazukin,[†] Peter C. Junk,*[,§] Berthold Kersting,[⊥] Stuart K. Langley,[†] Boujemaa Moubaraki,[†] Keith S. Murray,[†] Frederik Schleife,[⊥] Mahasish Shome,[†] David R. Turner,*[,†] and Julia A. Walker[†]

[†]School of Chemistry, Monash University, Clayton, Victoria 3800, Australia

[‡]School of Chemistry, The University of Manchester, Manchester M13 9PL, United Kingdom

[§]School of Pharmacy and Molecular Sciences, James Cook University, Townsville QLD 4811, Australia

[⊥]Institut für Anorganische Chemie, Universität Leipzig, Johannisallee 29, D-04103 Leipzig, Germany

S *Supporting Information*

ABSTRACT: Three complexes of the form $[Ln^{III}_3(OQ)_9]$ (Ln = Gd, Tb, Dy; OQ = 8-quinolinolate) have been synthesized and their magnetic properties studied. The trinuclear complexes adopt V-shaped geometries with three bridging 8-quinolinolate oxygen atoms between the central and peripheral eight-coordinate metal atoms. The magnetic properties of these three complexes differ greatly. Variable-temperature direct-current (dc) magnetic susceptibility measurements reveal that the gadolinium and terbium complexes display weak antiferromagnetic nearest-neighbor magnetic exchange interactions. This was quantified in the isotropic gadolinium case with an exchangecoupling parameter of $J = -0.068(2)$ cm^{-1}. The dysprosium compound displays weak ferromagnetic exchange. Variable-frequency and -temperature alternating-current magnetic susceptibility measurements on the anisotropic cases reveal that the dysprosium complex displays single-molecule-magnet behavior, in zero dc field, with two distinct relaxation modes of differing time scales within the same molecule. Analysis of the data revealed anisotropy barriers of U_{eff} = 92 and 48 K for the two processes. The terbium complex, on the other hand, displays no such behavior in zero dc field, but upon application of a static dc field, slow magnetic relaxation can be observed. Ab initio and electrostatic calculations were used in an attempt to explain the origin of the experimentally observed slow relaxation of the magnetization for the dysprosium complex.
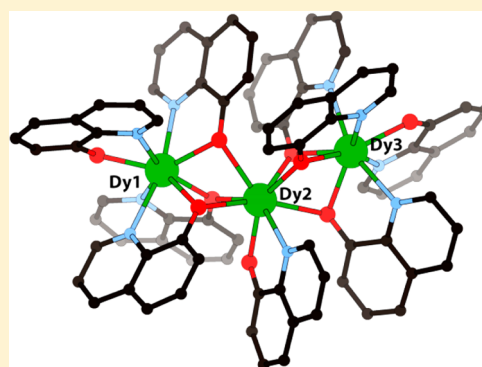
■ INTRODUCTION

Single-molecule-magnet (SMM) behavior refers to the ability of metal complexes to act as nanoscale magnets, typically at very low temperatures, by blocking the reversal of magnetization. The blocking of such magnetic moments is defined by an anisotropy barrier U_{eff}, the energy required to convert the molecule back to a paramagnet, with larger barriers leading to longer relaxation times. Slow-relaxing species such as these display magnetic memory effects and may potentially be useful as high-density information-storage media.[1] Furthermore, this behavior stems directly from the intrinsic properties of the electronic structure of the molecule itself; therefore, quantum effects such as quantum tunneling of the magnetization (QTM) are observable. Further applications based upon these quantum effects, such as quantum information processing, have also been proposed.[2−4] Historically, this behavior has been associated with transition-metal complexes, particularly those incorporating manganese or iron. Over the past decade, there has been an explosion of interest in the magnetic properties of the lanthanoid elements[5−7] both within clusters containing magnetically coupled ions and as isolated ions in mononuclear

complexes.[8,9] There has been particular interest in complexes of dysprosium because of its high anisotropy and the Kramers nature of the ion, which guarantees a doubly degenerate ground state.[10] Of particular relevance to the current work is a recent trinuclear dysprosium complex containing the 3-methyloxysalicylaldoxime ligand, as the complex has structural similarities to the Dy$_3$ species reported herein.[11]

Our recent work has explored the coordination chemistry and reactivity of 8-hydroxyquinoline (or 8-quinolinol, HOQ). The 8-quinolinolate anions (OQ$^-$) and related species, such as 2-methyl-8-hydroxyquinolinolate (MQ), are primarily known for their use as strong chelating agents in laboratory-based metal analysis,[12] within organic light-emitting diodes (as aluminum complexes) and as therapeutic reagents for metal chelation.[13−15] We have reported the use of high-temperature syntheses to isolate a number of alkali-metal, transition-metal, and rare-earth (mainly heterobimetallic) complexes of both the OQ and MQ anions as well as a number of heterometallic

species.[16−20] These complexes are made either by direct reaction of the elemental metal(s) with HOQ or by isolation of the $M(OQ)_n$ compound(s) with subsequent high-temperature rearrangement reactions. The homometallic rare-earth quinolinolate precursors are initially isolated as amorphous compounds, and only three examples have been structurally characterized; $[Er_3(OQ)_9]\cdot MeCN$ was obtained from acetonitrile,[21] $[Ho_3(OQ)_9]\cdot HOQ$ formed from an elevated temperature synthesis with holmium and strontium metals,[22] and $[Sc_2(OQ)_6]$ was prepared from $[Sc(N(SiMe_3)_2)_3]$ and HOQ.[23]

Herein we report the synthesis and structural characterization of the homoleptic compounds $[Ln^{III}_3(OQ)_9]$, where Ln = Gd, Tb, or Dy, and report their magnetic behavior with emphasis on exchange coupling and SMM behavior (Tb and Dy).

■ RESULTS AND DISCUSSION

Synthesis and Structure. The synthesis of quinolinolate complexes containing rare-earths complexes at elevated temperatures (>200 °C) has previously been reported.[17−20] Initially, using this method, the amorphous precursor material, $[Ln(OQ)_3]_n$, is isolated from the aqueous reaction of NaOQ with $LnCl_3$ to produce a noncrystalline material with a confirmed empirical composition of $[Ln(OQ)_3]^{12}$ but an unknown speciation (Scheme 1). It has now been found that

Scheme 1. Synthesis of Crystalline Complexes of the Type $[Ln_3(OQ)_9]$ (Ln = Gd, Tb, Dy)
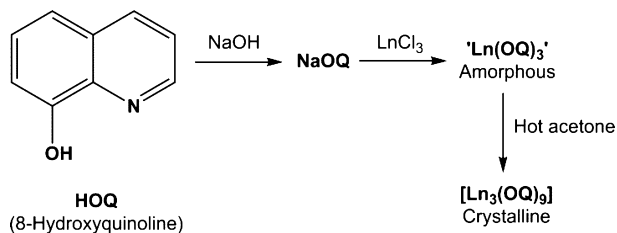
the sparingly soluble material can be sufficiently dissolved in hot acetone by Soxhlet extraction over the course of several days to yield a pure, microcrystalline material of the form $[Ln_3(OQ)_9]$ (Ln = Dy, Gd, Tb). Of particular note, the amorphous "$[Gd(OQ)_3]$" was transformed into crystalline $[Gd_3(OQ)_9]$ in the Soxhlet cup, with powder X-ray diffraction (PXRD) showing gradual improvement in crystallinity over this time (see the Supporting Information, Figure S1). IR spectra show that each compound is initially isolated as an acetone solvate. Microanalyses show loss of acetone, slightly for dysprosium and completely for gadolinium, with these losses being confirmed by IR spectroscopy. Thermogravimetric analyses (TGA) on fresh samples of the dysprosium and terbium compounds confirm the degree of solvation to be two acetone molecules per trinuclear complex. After being heated for 2 h under vacuum at 85 °C, the dysprosium sample could be almost completely desolvated, as indicated by IR spectroscopy, showing a substantially diminished band corresponding to the carbonyl absorption and no absorption characteristic of any hydration occurring. PXRD confirms that desolvation causes no structural changes compared to the solvated sample. Small crystals of the dysprosium analogue, of suitable quality to allow structural characterization by X-ray diffraction using a synchrotron light source, were deposited from acetone (see the Experimental Section). PXRD confirmed that the three

materials are isomorphous, with diffraction-quality single crystals unobtainable for the gadolinium and terbium analogues (see the Supporting Information, Figure S2). The complexes are isomorphous with $[Er_3(OQ)_9]\cdot MeCN^{21}$ but not with $[Ho_3(OQ)_9]\cdot HOQ.^{22}$

The compound $[Dy_3(OQ)_9]$ crystallizes in the triclinic space group $P\bar{1}$, with the entire complex and approximately 1.7 acetone molecules contained within the asymmetric unit (Figure 1). The homoleptic, trinuclear complex adopts a "V-
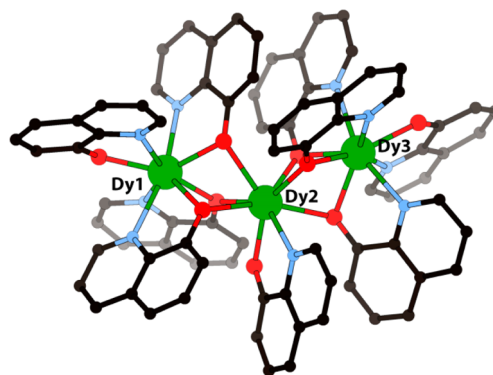

Figure 1. Structure of the trinuclear complex $[Dy_3(OQ)_9]$ as determined by X-ray crystallography. Disorder of two OQ ligands, H atoms and acetone of crystallization are not shown for clarity.

shaped" geometry of the three Dy ions with a Dy···Dy···Dy angle of 134°. The Dy···Dy separations are both 3.52 Å. All three Dy centers are eight-coordinate with a mixture of chelating and μ-$1\kappa(N,O):2\kappa(O)$ bridging OQ ligands. The two terminal Dy ions have the same coordination sphere; four chelating OQ ligands surround the metal, three of which bridge the central Dy ion by μ_2-quinolinolate O atoms, giving these ions an N_4O_4 coordination environment. The central Dy atom is coordinated by six O atoms from the bridging OQ ligands in addition to one chelating OQ ligand, giving overall NO_7 coordination. The chelating ligand on the central metal is disordered over two positions, with the coordinating O and N atoms being swapped in the two orientations. The Dy−O distances associated with purely chelating ligands are shorter than those involving μ_2-O atoms with distances in the ranges 2.241(6)−2.30(2) and 2.313(3)−2.476(3) Å, respectively. The chelate angle itself does not appear to be dependent on the overall coordination mode of the ligand, with all N−Dy−O angles lying in the range 65.1(10)−68.435(11)°. For all but one of the bridging ligands, the Dy−O distance within the chelate is shorter than that to the central Dy ion, while for the remaining chelating ligand, the two distances are the same within error. The Dy−N distances are significantly longer than the Dy−O lengths and lie in the range 2.490(4)−2.613(9) Å. The Dy−O− Dy angles subtended at the bridging phenolate O atom lie in the range 94.54(10)−97.82(10)°. Examining the dysprosium coordination polyhedra with the *SHAPE* software[24] reveals that the terminal Dy sites (Dy1 and Dy3) are of distorted triangular dodecahedral geometry, with continual shape measures (CShMs) of ~1.64 and 1.59, respectively. The central Dy2, however, resides in a site of distorted square-antiprismatic (SAP) geometry, with a CShM of ~1.62. The structure packs predominantly through face-to-face π interactions, with the solvent residing in pockets between the complexes with no strong intermolecular interactions (see the Supporting Information, Figure S3).

Magnetic Susceptibility Measurements. Direct-current (dc) magnetic susceptibility measurements were performed on polycrystalline samples of $[Gd_3(OQ)_9]$, $[Tb_3(OQ)_9]$, and $[Dy_3(OQ)_9]$, using applied magnetic fields of 0.02, 0.1, and 1 T in the temperature range 2−300 K. The $\chi_M T$ values at room temperature for $[Gd_3(OQ)_9]$, $[Tb_3(OQ)_9]$, and $[Dy_3(OQ)_9]$ are found to be 24.35, 35.59, and 39.56 cm^3 K mol^{-1}, respectively (Figure 2). In each case, this value is close to that
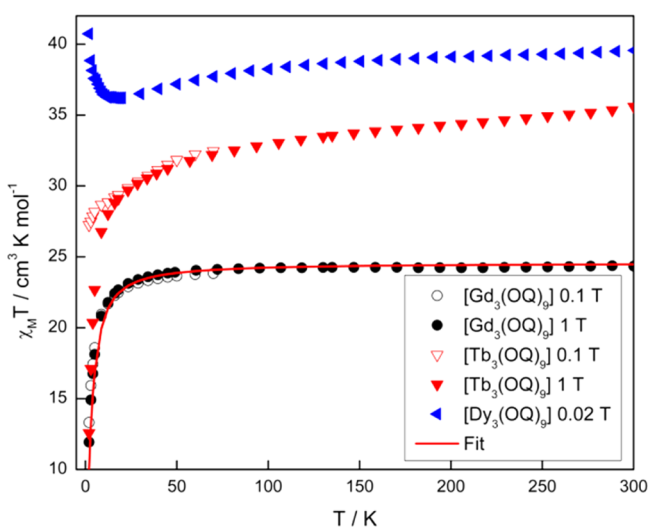

Figure 2. $\chi_M T$ versus temperature for $[Gd_3(OQ)_9]$, $[Tb_3(OQ)_9]$ and $[Dy_3(OQ)_9]$ in applied magnetic fields of 0.02, 0.1, and 1 T. The solid red line is a fit of the $[Gd_3(OQ)_9]$ 1 T experimental data using the parameters given in the text.

expected for three noninteracting Gd^{III} ($^8S_{7/2}$, $g = 2$), Tb^{III} ($^7F_6$, $g = {}^3/_2$), and Dy^{III} ($^6H_{15/2}$, $g = {}^4/_3$) ions of 23.63, 35.46, and 42.51 cm^3 K mol^{-1}. These values indicate that the magnetic exchange is weak as expected because of the shielded nature of the 4f orbitals. The $\chi_M T$ product for the $[Gd_3(OQ)_9]$ complex remains constant upon reduction of the temperature to ∼50 K, where the value begins to decrease gradually, before a more rapid decrease below 20 K, reaching a value of 11.92 cm^3 K mol^{-1} at 2 K and 1 T. This temperature dependence indicates weak antiferromagnetic exchange between the Gd^{III} ions, although zero-field splitting and Zeeman level depopulation

may also be contributing to the behavior. The isothermal M versus H plots for the gadolinium(III) complex (Supporting Information, Figure S4) show that at 2 K the magnetization is close to saturation with a value of $M = 21.2\ \mu_B$ at 5 T. In an attempt to quantify the magnetic interactions, we modeled both the $\chi_M T$ versus T and M versus H data simultaneously, using a one J coupling scheme, with only the nearest-neighbor interactions considered. Using the spin Hamiltonian $\hat{H} = -2J(\hat{S}_1\hat{S}_2 + \hat{S}_2\hat{S}_3) + g\mu_B B(\hat{S}_1 + \hat{S}_2)$ within the program PHI,[25] we determined the exchange coupling constant to be $J = -0.068(2)$ cm^{-1}, with a g value of 2.04(1). With these parameters, the ground spin state is found to be $S = {}^7/_2$, with the first excited state ($S = {}^5/_2$) 0.48(2) cm^{-1} above the ground, with the entire energy spectrum of spin states falling within 7.2(3) cm^{-1} of the ground state. The fits are shown as red lines in Figures 2 and S4 (see the Supporting Information). The exchange is thus confirmed to be antiferromagnetic and extremely weak, as observed in the majority of gadolinium(III) complexes.[26,27]

The temperature dependence of the $[Tb_3(OQ)_9]$ complex reveals a constant decrease in $\chi_M T$ upon lowering of the temperature, reaching a value of 12.57 cm^3 K mol^{-1} at 2 K and 1 T. This is attributable to a gradual depopulation of the m_J sublevels of the ground J multiplet, with the likelihood of antiferromagnetic exchange and/or dipolar coupling also contributing to the behavior. A small field dependence is also found, with the low-temperature $\chi_M T$ profiles diverging at differing fields. The $\chi_M T$ temperature dependence for the $[Dy_3(OQ)_9]$ compound is substantially different, however, with an upturn in $\chi_M T$ observed below 18 K, reaching a value of 40.73 cm^3 K mol^{-1} at 2 K. While the high-temperature behavior is similar to that of the terbium(III) analogue, the small low-temperature increase suggests that weak ferromagnetic exchange is present between the Dy^{III} ions. It must be noted that ferromagnetic exchange between Dy^{III} ions is still relatively uncommon.[28−32]

The isothermal M versus H plots for $[Tb_3(OQ)_9]$ and $[Dy_3(OQ)_9]$ do not saturate at 2 K in fields ranging from 0 to 5 T, reaching values of 13.19 and 14.85 Nβ, respectively. These values are lower than expected for three free Tb^{III} and Dy^{III} ions again because of crystal-field effects eliminating the degeneracy of the ground J multiplet (see the Supporting Information, Figures S5 and S6).
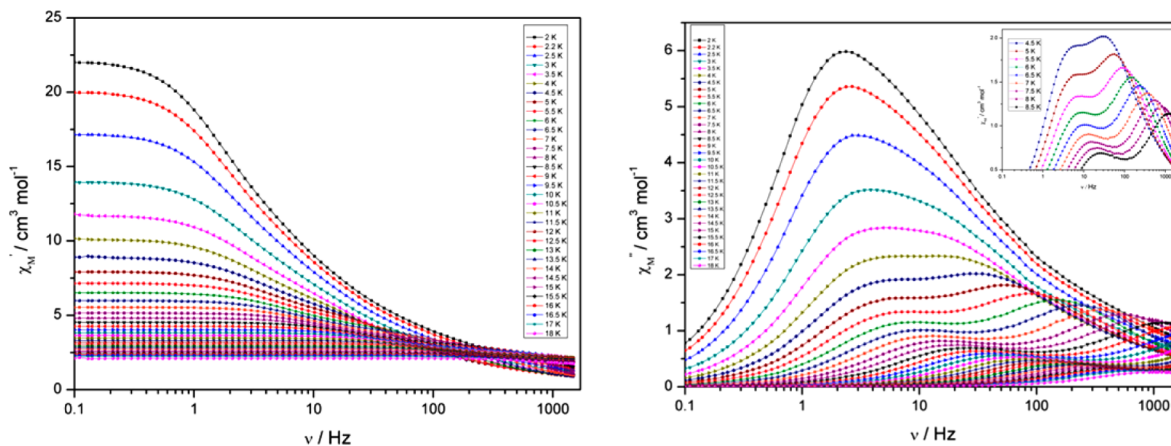

Figure 3. Frequency dependence of χ_M' (left) and χ_M'' (right) for $[Dy_3(OQ)_9]$ at temperatures between 2 and 18 K, with a 3.5 Oe ac field and a zero applied dc field. The inset highlights the double maxima observed in χ_M'' for the sample.

Alternating-current (ac) magnetic susceptibility measurements were performed on the anisotropic complexes $[Tb_3(OQ)_9]$ and $[Dy_3(OQ)_9]$ to check for the presence of any slow magnetic relaxation. The results reveal significantly different features for each complex. The $[Dy_3(OQ)_9]$ analogue displays both a frequency and temperature dependence in both the in-phase (χ_M') and out-of-phase (χ_M'') susceptibility, in zero dc field (Figure 3) indicative of SMM behavior, while the $[Tb_3(OQ)_9]$ complex displays no such behavior.

Focusing on the dysprosium(III) complex, the χ_M'' versus frequency plot clearly displays two separate peak maxima in χ_M'', over a range of temperatures indicating that two relaxation modes are occurring with differing relaxation time scales (Figure 3, right). Because the relaxation time at the peak maxima is inversely proportional to the frequency, then at a single temperature in the χ_M'' versus frequency plot the peak maxima observed at the lower frequency denote a slower relaxation time, and thus we designate this as the slow process (SP). The higher-frequency peak (faster relaxation time) is denoted as the fast process (FP). This is observed clearly at temperatures between 4.5 and 8.5 K and is highlighted in Figure 3 (right, inset). Isothermal Cole–Cole diagrams reveal two fused semicircular profiles below 8.5 K, indicating that two separate relaxation processes are in operation, and above this temperature the second, faster process moves out of the time scale of the experiment. Fits of the Cole–Cole data between 3.5 and 18 K using a generalized Debye model revealed that, across the entire temperature range, the SP has an extremely narrow distribution of relaxation times, where $\alpha \approx 0$. Conversely, the FP has a larger distribution of relaxation times, where α increases from 0.2 to 0.4 as the temperature is lowered from 8 to 3.5 K (Figure 4, inset). Plots of $\ln(\tau)$ versus T^{-1} (Figure 4) are linear above 13.5 and 6.5 K for the SP and FP, respectively, revealing a thermally activated relaxation mechanism. Fittings of the Arrhenius law $[\tau = \tau_0 \exp(U_{eff}/k_B T)]$ afforded values of $U_{eff} = 92 \pm 2$ K and $\tau_0 = 1.02 \times 10^{-6}$ s (SP) and $U_{eff} = 48 \pm 2$ K and $\tau_0 = 5.57 \times 10^{-7}$ s (FP). Below these temperatures, deviations from Arrhenius behavior are observed as a curvature
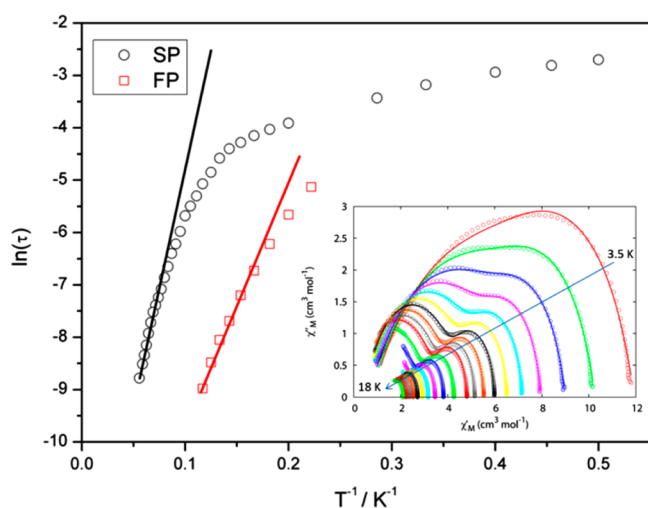
in the plot, for both pathways, indicating a crossover from a thermally activated to a quantum-tunneling mechanism of relaxation. This behavior is more clearly observed for the SP because the relaxation time becomes close to being independent of temperature below 3 K, while $\chi_M''_{max}$ for the FP is obscured by the SP and thus no low-temperature relaxation times could be extracted. It is found, however, that the SP displays a tunneling rate of ~2.3 Hz, relating to a relaxation time of 67.2 ms.

In order to explore whether solvation of polycrystalline $[Dy_3(OQ)_9]$, by acetone or water, played a part in the double maxima observed in the χ_M'' versus frequency plots of Figure 3 and hence in the double relaxation behavior, we made a fresh polycrystalline sample, measured its TGA, and desolvated it by heating it in vacuo at 85 °C for 2 h. The solvated material showed the characteristic $\nu(C=O)$ band of acetone at 1700 cm^{-1}, while the desolvated sample showed a very weak band at this frequency with no bands indicative of water of solvation. The χ_M'' versus frequency plots (see the Supporting Information, Figure S7) were essentially identical for both samples and clearly indicative of the double maxima behavior, thus showing that the presence of acetone of crystallization plays no part in the susceptibility behavior.

It has been well established that SMM behavior originating from single-ion lanthanide complexes stems from interaction of the ground spin–orbit-coupled J state with the crystal field, resulting in an anisotropy barrier separating the opposite projections of the magnetic ground state.[33] Two essential conditions to achieve such behavior is for the ground state to be bistable, of high magnitude $\pm m_J$ quantum number and with a large separation between the ground and first excited $\pm m_J$ states.[34] This has been found to be commonplace for dysprosium(III)-containing complexes, with many SMMs recently being reported.[7,35] While it appears that the relaxation mechanism(s) in lanthanoid-containing systems is (are) more complex than their transition-metal-based counterparts, it has been found that the ground to first excited state separation correlates in many cases to the height of the experimentally observed anisotropy barrier.[8] The subtle difference between unique coordination environments found in multinuclear complexes can lead to very different local electronic structures, thus possibly leading to multiple relaxation processes within the same molecule. This is examined in more detail in the subsequent section.

While the $[Tb_3(OQ)_9]$ complex displayed no observable out-of-phase signal when measurements were taken in zero dc field (Figure 5, left), performing the measurement in a 5000 Oe applied dc field revealed frequency-dependent maxima in the plot of χ_M'' versus T, indicating field-induced SMM behavior (Figure 5, right). This commonly observed feature for terbium(III)-based complexes is due to fast zero-field tunneling of the magnetization between sublevels, due to the non-Kramers nature of the ion. This allows for the direct mixing of opposing projections of the ground-state angular momentum by the crystal field, such that tunneling pathways are often readily available. This is contrary to Dy^{III}, which is a Kramers ion, and thus the requirement of a bistable ground state, as is necessary for SMM behavior, is met irrespective of the symmetry of the coordination environment.

Ab Initio and Electrostatic Calculations. In order to better understand the character of the slow magnetic relaxation of the Dy complex, ab initio calculations of the CASSCF/CASSI type were performed with *MOLCAS 7.8*.[36−38] The
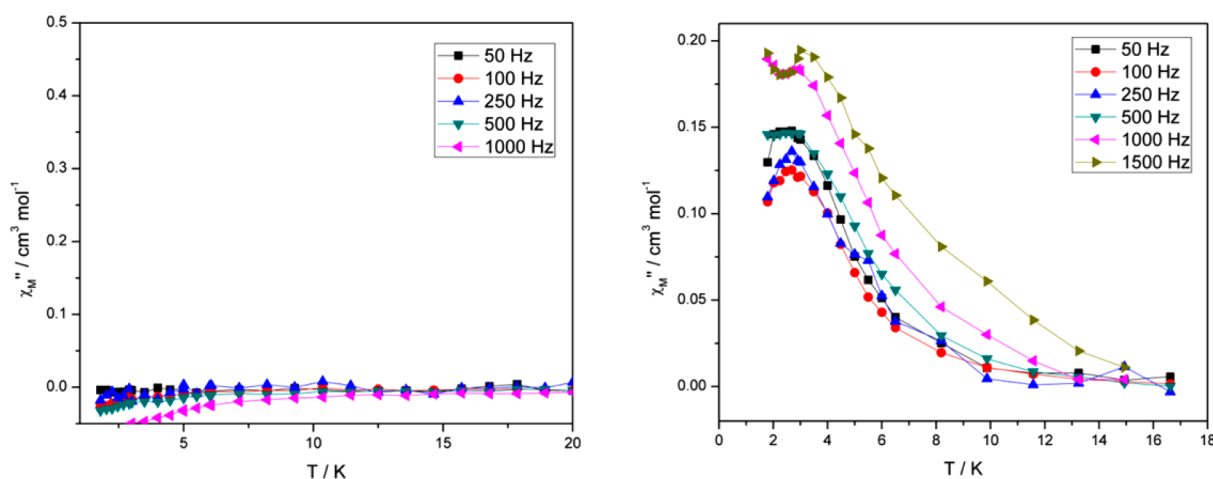

Figure 4. Magnetization relaxation time (τ) plotted as $\ln(\tau)$ versus T^{-1} for $[Dy_3(OQ)_9]$. The solid black and red lines represent a fit to the Arrhenius law in the thermally activated regime for the SP and FP, respectively. (inset) Cole–Cole plots of $[Dy_3(OQ)_9]$ at temperatures between 3.5 and 18 K. The solid lines are fits of the experimental data using a generalized Debye model.

Figure 5. Temperature dependence of χ_M'' for $[Tb_3(OQ)_9]$ in a (left) zero applied dc field, with an ac field of 3.5 Oe and (right) under a 5000 Oe applied dc field and a 3.5 Oe ac field.

structure of $[Dy_3(OQ)_9]$ determined by X-ray diffraction was used directly where the arrangement of the major component of the disordered ligands was employed. Calculations were performed for each Dy^{III} site independently (Dy^{III} atoms not of interest were replaced by Lu^{III}), where the active space was in all cases nine electrons in seven orbitals. Because of computational limitations, only 21 sextets and 128 quartets were mixed by spin−orbit coupling. The ANO-RCC basis sets were used exclusively, where the Dy^{III} ion of interest was of VTZP quality, the first coordination sphere of VDZP quality, and all other atoms of VDZ quality. The resultant energy levels and **g** tensors for the $^6H_{15/2}$ multiplets for each site are given in Tables 1−3.

Table 1. Electronic Properties for Dy1

E (cm^{-1})	g_x	g_y	g_z	angle (deg)
0.0	0.01	0.02	19.55	
106.1	0.07	0.08	17.07	14.0
225.0	0.02	0.12	14.29	19.7
326.4	0.95	1.39	10.40	11.8
395.5	4.70	6.32	9.53	63.1
457.8	1.14	1.73	16.41	81.6
559.2	0.18	0.57	17.19	76.1
614.8	0.19	0.85	18.27	76.7

Table 2. Electronic Properties for Dy2

E (cm^{-1})	g_x	g_y	g_z	angle (deg)
0.0	0.00	0.01	19.61	
114.9	0.08	0.11	16.76	5.5
214.7	0.09	0.22	14.50	34.2
274.8	1.79	2.19	10.58	38.6
326.8	5.05	6.28	8.39	83.2
359.9	0.47	1.73	15.93	88.9
398.7	0.47	1.26	16.57	80.6
638.2	0.01	0.01	19.78	69.0

Broadly, the energy spectra of each site are similar, with first excited states of 96−115 cm^{-1} and the multiplets spanning 541−638 cm^{-1}. The ground-state **g** tensors are all strongly axial, approaching the Ising limit of $g_x = g_y = 0$ and $g_z = 20$, corresponding to the state $m_J = {}^{15}/_2$ of Dy^{III}. Because the ground states in these low-symmetry environments are very

Table 3. Electronic Properties for Dy3

E (cm^{-1})	g_x	g_y	g_z	angle (deg)
0.0	0.02	0.04	19.65	
96.0	0.21	0.26	16.90	3.8
194.8	0.57	0.79	13.69	2.1
258.6	4.29	4.59	9.39	18.4
321.1	0.71	4.93	9.77	83.6
378.1	2.05	3.00	14.95	80.2
494.5	0.04	0.51	17.94	77.9
540.7	0.10	0.61	18.63	80.3

close to $m_J = {}^{15}/_2$, we can employ an electrostatic minimization of the $\rho_{\pm 15/2}$ Sievers electron density,[39] in order to understand the ab initio magnetic anisotropy axes. This homoleptic complex can be easily described in the minimal valence bond (VB) framework, outlined in ref 39, where each Dy^{III} ion has a 3+ charge, the O atoms all possess a 1− charge, and all other atoms are neutral. For Dy1 and Dy3, the electrostatic environment is best described as an axially compressed trigonal pyramid, composed of the negatively charged O atoms, supported by a ring of four neutral N atoms. The apical O atom from the chelating OQ^- ligand is substantially closer to each Dy1 and Dy3 than the other O atoms [2.272(4) Å compared to 2.34(3) Å], leading to an axially repulsive potential for the oblate $\rho_{\pm 15/2}$ electron density. This defines the orientation of the ground-state magnetic anisotropy, in excellent agreement with the ab initio calculations, where the deviations between the electrostatic and ab initio anisotropy axes are 9.8 and 4.0° for Dy1 and Dy3, respectively (Figure 6). Although the central Dy2 possesses a different coordination sphere and geometry, the chelating OQ^- ligand is similarly found to have a substantially shorter Dy−O bond at 2.241(6) Å compared to 2.39(6) Å, which is again responsible for driving the magnetic anisotropy, as elucidated with the ab initio calculations, where the electrostatic ab initio deviation is 8.9° (Figure 5). While we were not able to perform ab initio calculations on the minor disordered conformation because of its low crystallography occupancy and precision, it is expected that the orientation of the magnetic anisotropy would be altered because of the flipping of the chelating OQ^- ligand.

A small ferromagnetic interaction between the three Dy^{III} ions (likely ≪1 cm^{-1} because of the sub-18 K increase in $\chi_M T$) would cause a set of exchange Kramers doublets split over a

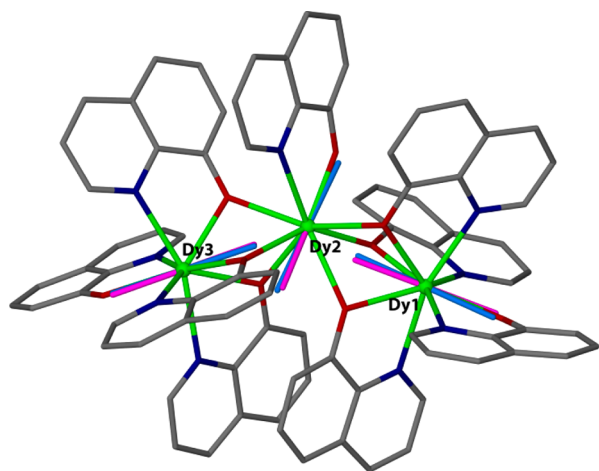**Figure 6.** Magnetic anisotropy axes for $[Dy_3(OQ)_9]$. Blue rods are from ab initio calculations, while pink rods are from electrostatic calculations. H atoms are omitted for clarity.

range on the order of exchange energy, with the first set of well-separated excited states around the energy of the free-ion first excited states, around 100 cm^{-1}. Thus, it is possible that the SP pathway involves either one or some of the free-ion excited states or one of the exchange states. Unfortunately, we are not able to rationalize the origin of the FP because its energy does not correspond to a free-ion state, and for an exchange state to have such an energy, the magnetic interaction would have to be much stronger.

CONCLUSIONS

The isostructural series of homoleptic, trinuclear lanthanoid complexes $[Ln_3(OQ)_9]$ (Ln = Dy, Gd, Tb) has been synthesized and characterized, and the magnetic and electronic properties have been examined. The variable-temperature magnetic susceptibility of the isotropic $[Gd_3(OQ)_9]$ complex was modeled using a single-exchange coupling constant, revealing weak antiferromagnetic behavior. Contrary to this, the $[Dy_3(OQ)_9]$ complex displayed weak ferromagnetic exchange. ac susceptibility measurements allowed for the dynamics of the magnetization to be evaluated for the anisotropic complexes. The $[Tb_3(OQ)_9]$ compound displayed an absence of any out-of-phase peaks (χ_M'') in zero applied dc field; however, upon application of a 5000 Oe dc field, slow relaxation was observed. This is most likely due to the action of the small magnetic field either preventing QTM mechanisms or overcoming the exchange interaction bias. On the other hand, the $[Dy_3(OQ)_9]$ complex clearly shows slow relaxation in zero dc field. Two distinct relaxation pathways can be observed, with anisotropy barriers of U_{eff} = 92 and 48 K for the SP and FP, respectively, operating on differing time scales, the origins of which cannot be fully elucidated at this time. The OQ ligand has thus proven to be effective in the formation of homoleptic complexes that are capable of showing SMM behavior.

EXPERIMENTAL SECTION

Synthesis. All reagents and solvents were purchased from standard commercial suppliers and used without further purification. Amorphous materials of $[Ln(OQ)_3]_n$ were synthesized according to previously reported methods by the reaction of LnCl$_3$·6H$_2$O with NaOQ in ethanol.[18] Microanalyses were conducted at the Campbell Analytical Laboratories, University of Otago, Dunedin, New Zealand or the London Metropolitan University. PXRD data were collected

using a Bruker AXS D8 diffractometer equipped with Cu Kα radiation and operating at room temperature. TGAs were carried out using a Mettler STARe system at a heating rate of 5 °C min^{-1} under a stream of dry N$_2$ gas.

[Dy$_3$(OQ)$_9$]. The crude material $[Dy(OQ)_3]_n$ (0.70 g, 1.2 mmol) was placed in a Soxhlet thimble and extracted with acetone for 36 h. After this time, the acetone was cooled and left to evaporate, leaving a yellow microcrystalline product of the compound as an acetone solvate (from single-crystal data), $[Dy_3(OQ)_9]$·1.76(CH$_3$)$_2$CO (0.12 g, 29%). Microanal. Calcd for C$_{86.28}$H$_{64.56}$Dy$_3$N$_9$O$_{10.76}$ ($[Dy_3(OQ)_9]$·1.76-(CH$_3$)$_2$CO): C, 54.92; H, 3.45; N, 6.68. Found: C, 54.29; H, 3.70; N, 6.24. PXRD of bulk material confirms the presence of a single, crystalline material (see the Supporting Information). IR (ATR, $\tilde{\nu}$/cm^{-1}): 1703 (m), 1597 (m), 1566 (s), 1494 (s), 1459 (vs), 1430 (m), 1378/1370 (s, br), 1318 (vs), 1273 (m), 1228 (m), 1104 (vs), 1032 (w), 821 (s), 792 (m), 786 (s), 727 (vs). Mp: 300−304 °C. TGA: 70−250 °C, 6.1% weight loss (calculated 6.1% for two acetone molecules per trinuclear complex). TGA/microanalysis suggests that the acetone of solvation is readily lost.

[Gd$_3$(OQ)$_9$]. The crude material $[Gd(OQ)_3]_n$ (0.52 g, 0.83 mmol) was placed in a Soxhlet thimble and extracted with acetone for 7 days. After this time, the acetone was cooled and left to evaporate, leaving a yellow microcrystalline product (0.15 g, 32%). Microanal. Calcd for C$_{81}$H$_{54}$Gd$_3$N$_9$O$_9$ ($[Gd_3(OQ)_9]$, no acetone of crystallization): C, 54.99; H, 3.07; N, 7.12. Found: C, 54.83; H, 3.13; N, 7.07. PXRD confirms a pure crystalline compound, isostructural with the Dy analogue (see the Supporting Information). IR (ATR, $\tilde{\nu}$/cm^{-1}): 1700 (vw), 1595 (w), 1570 (s), 1494 (vs), 1461 (vs), 1422 (w), 1379 (s, br), 1314 (vs), 1274 (s), 1232 (w), 1103 (vs), 1034 (w), 821 (s), 800 (m), 786 (s), 740 (m), 727 (vs). Mp: 300−310 °C.

[Tb$_3$(OQ)$_9$]. The crude material $[Tb_3(OQ)_3]_n$ (0.50 g, 0.80 mmol) was placed in a Soxhlet thimble and extracted with acetone for 3 days. After this time, the acetone was cooled and left to evaporate, leaving a yellow microcrystalline product (0.14 g, 30%). Microanal. Calcd for C$_{87}$H$_{66}$N$_9$O$_{11}$Tb$_3$ ($[Tb_3(OQ)_9]$·2Me$_2$CO): C, 55.27; H, 3.49; N, 6.67. Found: C, 54.87; H, 3.07; N, 7.11. PXRD confirms a pure crystalline compound, isostructural with the Dy analogue (see the Supporting Information). IR (ATR, $\tilde{\nu}$/cm^{-1}) = 1703 (m, br), 1593 (m), 1562 (s), 1490 (s), 1459 (vs), 1428 (m), 1387/1365 (s, br), 1315 (vs), 1272 (s), 1227 (m), 1103 (vs), 823 (s), 785 (s), 727 (vs). Mp: 300−310 °C. TGA: 70−250 °C, 6.0% weight loss (calculated 6.1% for two acetone per trinuclear complex).

X-ray Crystallography. Data were collected using the MX1 beamline at the Australian Synchrotron operating at 17.4 keV (λ = 0.7107 Å). The data collection temperature was maintained at 100 K using an open-flow N$_2$ cryostream. Data collection was conducted using the program *BluIce*.[40] Initial data reduction was carried out using the *XDS* package.[41] The structure was solved by direct methods using *SHELXS-97*.[42] Least-squares refinement against F^2 was conducted using *SHELXL-2013* using the program *X-Seed* as a graphical interface.[43] All non-H atoms were refined using an anisotropic model. H atoms were placed in idealized positions and refined using riding models. The structure contains disorder of two OQ ligands and a partial occupancy acetone molecule (whose occupancy is related to one of the disordered ligands). Full refinement details are provided in the Supporting Information. Crystallographic data for this compound have been deposited with the Cambridge Crystallographic Data Centre (no. 966476).

Crystal data for $[Dy_3(OQ)_9]$·1.76(CH$_3$)$_2$CO: C$_{86.27}$H$_{64.54}$Dy$_3$N$_9$O$_{10.76}$, M = 1886.83, yellow block, 0.03 × 0.03 × 0.02, space group $P\bar{1}$ (No. 2), V = 3594.7(13) Å^3, Z = 2, D_c = 1.743 g cm^{-3}, F_{000} = 1858, $2\theta_{max}$ = 57.2°, 63106 reflections collected, 16492 unique (R_{int} = 0.0317). Final GOF = 1.078, R1 = 0.0349, wR2 = 0.0894, R indices based on 14972 reflections with $I > 2\sigma(I)$, 1196 parameters, 75 restraints, μ = 3.158 mm^{-1}.

Magnetic Susceptibility Measurements. The magnetic susceptibility measurements were carried out on a Quantum Design SQUID MPMS-XL 7 magnetometer operating between 1.8 and 300 K for dc applied fields ranging from 0 to 5 T. Samples were dispersed in Vaseline in order to avoid torquing of the crystallites. The sample

mulls were contained in a calibrated gelatin capsule held at the center of a drinking straw that was fixed at the end of the sample rod. ac susceptibilities were carried out under an oscillating ac field of 3.5 Oe and frequencies ranging from 0.1 to 1500 Hz.

■ ASSOCIATED CONTENT

ⓢ Supporting Information

X-ray crystallographic data in CIF format, full crystallographic refinement details, PXRD data of $[Dy_3(OQ)_9]$ crystallization over 7 days, and additional magnetic plots. This material is available free of charge via the Internet at http://pubs.acs.org.

■ AUTHOR INFORMATION

Corresponding Authors
*E-mail: david.turner@monash.edu (D.R.T.).
*E-mail: peter.junk@jcu.edu.au (P.C.J.).

Notes
The authors declare no competing financial interest.

■ ACKNOWLEDGMENTS

■ REFERENCES

(1) Mannini, M.; Pineider, F.; Sainctavit, P.; Danieli, C.; Otero, E.; Sciancalepore, C.; Talarico, A. M.; Arrio, M.-A.; Cornia, A.; Gatteschi, D.; Sessoli, R. *Nat. Mater.* **2009**, *8*, 194−197.

(2) Ardavan, A.; Rival, O.; Morton, J. J. L.; Blundell, S. J.; Tyryshkin, A. M.; Timco, G. A.; Winpenny, R. E. P. *Phys. Rev. Lett.* **2007**, *98*, 057201.

(3) Aromi, G.; Aguila, D.; Gamez, P.; Luis, F.; Roubeau, O. *Chem. Soc. Rev.* **2012**, *41*, 537−546.

(4) Leuenberger, M. N.; Loss, D. *Nature* **2001**, *410*, 789−793.

(5) Luzon, J.; Sessoli, R. *Dalton Trans.* **2012**, *41*, 13556−13567.

(6) Sessoli, R.; Powell, A. K. *Coord. Chem. Rev.* **2009**, *253*, 2328−2341.

(7) Woodruff, D. N.; Winpenny, R. E. P.; Layfield, R. A. *Chem. Rev.* **2013**, *113*, 5110−5148.

(8) Chilton, N. F.; Langley, S. K.; Moubaraki, B.; Soncini, A.; Batten, S. R.; Murray, K. S. *Chem. Sci* **2013**, *4*, 1719−1730.

(9) Williams, U. J.; Mahoney, B. D.; DeGregorio, P. T.; Carroll, P. J.; Nakamaru-Ogiso, E.; Kikkawa, J. M.; Schelter, E. J. *Chem. Commun.* **2012**, *48*, 5593−5595.

(10) Kramers, H. A. *Proc. R. Acad. Sci. Amsterdam* **1930**, *33*, 959−972.

(11) Guo, F. S.; Liu, J. L.; Leng, J. D.; Meng, Z. S.; Lin, Z. J.; Tong, M. L.; Gao, S.; Ungur, L. V.; Chibotaru, L. F. *Chem.—Eur. J* **2011**, *17*, 2458−2466.

(12) Hollingshead, R. G. W. *Oxine and Its Derivatives*; Butterworth: London, 1954; Vol. *I*.

(13) Opazo, C.; Luza, S.; Villemagne, V. L.; Volitakis, I.; Rowe, C.; Barnham, K. J.; Strozyk, D.; Masters, C. L.; Cherny, R. A.; Bush, A. I. *Aging Cell* **2006**, *5*, 69−79.

(14) Phillips, J. P. *Chem. Rev.* **1956**, *56*, 271−297.

(15) Tang, C. W.; Vanslyke, S. A. *Appl. Phys. Lett.* **1987**, *51*, 913−915.

(16) Deacon, G. B.; Junk, P. C.; Turner, D. R.; Walker, J. A. *Aust. J. Chem.* **2013**, *66*, 1138−1143.

(17) Deacon, G. B.; Dierkes, T.; Huebner, M.; Junk, P. C.; Lorenz, Y.; Urbatsch, A. *Eur. J. Inorg. Chem.* **2011**, 4338−4348.

(18) Deacon, G. B.; Forsyth, C. M.; Junk, P. C.; Kynast, U.; Meyer, G.; Moore, J.; Sierau, J.; Urbatsch, A. *J. Alloys Compd.* **2008**, *451*, 436−439.

(19) Deacon, G. B.; Forsyth, C. M.; Junk, P. C.; Urbatsch, A. *Eur. J. Inorg. Chem.* **2010**, 2787−2797.

(20) Deacon, G. B.; Junk, P. C.; Leary, S. G.; Urbatsch, A. *Z. Anorg. Allg. Chem.* **2012**, *638*, 2001−2007.

(21) Artizzu, F.; Deplano, P.; Marchio, L.; Mercuri, M. L.; Pilia, L.; Serpe, A.; Quochi, F.; Orru, R.; Cordella, F.; Meinardi, F.; Tubino, R.; Mura, A.; Bongiovanni, G. *Inorg. Chem.* **2005**, *44*, 840−842.

(22) Leary, S. G.; Deacon, G. B.; Junk, P. C. *Z. Anorg. Allg. Chem.* **2005**, *631*, 2647−2650.

(23) Katkova, M. A.; Balashova, T. V.; Pushkarev, A. P.; Ilyin, I. Y.; Fukin, G. K.; Baranov, E. V.; Ketkov, S. Y.; Bochkarev, M. N. *Dalton Trans.* **2011**, *40*, 7713−7717.

(24) Alvarez, S.; Alemany, P.; Casanova, D.; Cirera, J.; Llunell, M.; Avnir, D. *Coord. Chem. Rev.* **2005**, *249*, 1693−1708.

(25) Chilton, N. F.; Anderson, R. P.; Turner, L. D.; Soncini, A.; Murray, K. S. *J. Comput. Chem.* **2013**, *34*, 1164−1175.

(26) Langley, S. K.; Chilton, N. F.; Ungur, L.; Moubaraki, B.; Chibotaru, L. F.; Murray, K. S. *Inorg. Chem.* **2012**, *51*, 11873−11881.

(27) Sweet, L. E.; Roy, L. E.; Meng, F.; Hughbanks, T. *J. Am. Chem. Soc.* **2006**, *128*, 10193−10201.

(28) Guo, F.-S.; Liu, J.-L.; Leng, J.-D.; Meng, Z.-S.; Lin, Z.-J.; Tong, M.-L.; Gao, S.; Ungur, L.; Chibotaru, L. F. *Chem.—Eur. J* **2011**, *17*, 2458−2466.

(29) Guo, Y.-N.; Chen, X.-H.; Xue, S.; Tang, J. *Inorg. Chem.* **2011**, *50*, 9705−9713.

(30) Guo, Y.-N.; Xu, G.-F.; Wernsdorfer, W.; Ungur, L.; Guo, Y.; Tang, J.; Zhang, H.-J.; Chibotaru, L. F.; Powell, A. K. *J. Am. Chem. Soc.* **2011**, *133*, 11948−11951.

(31) Lin, P.-H.; Burchell, T. J.; Clerac, R.; Murugesu, M. *Angew. Chem., Int. Ed.* **2008**, *47*, 8848−8851.

(32) Xu, G.-F.; Wang, Q.-L.; Gamez, P.; Ma, Y.; Clerac, R.; Tang, J.; Yan, S.-P.; Cheng, P.; Liao, D.-Z. *Chem. Commun.* **2010**, *46*, 1506−1508.

(33) Ishikawa, N. *Polyhedron* **2007**, *26*, 2147−2153.

(34) Rinehart, J. D.; Long, J. R. *Chem. Sci* **2011**, *2*, 2078−2085.

(35) Zhang, P.; Guo, Y. N.; Tang, J. K. *Coord. Chem. Rev.* **2013**, *257*, 1728−1763.

(36) Aquilante, F.; De Vico, L.; Ferre, N.; Ghigo, G.; Malmqvist, P.-A.; Neogrady, P.; Pedersen, T. B.; Pitonak, M.; Reiher, M.; Roos, B. O.; Serrano-Andres, L.; Urban, M.; Veryazov, V.; Lindh, R. *J. Comput. Chem.* **2010**, *31*, 224−247.

(37) Karlstrom, G.; Lindh, R.; Malmqvist, P. A.; Roos, B. O.; Ryde, U.; Veryazov, V.; Widmark, P. O.; Cossi, M.; Schimmelpfennig, B.; Neogrady, P.; Seijo, L. *Comput. Mater. Sci.* **2003**, *28*, 222−239.

(38) Veryazov, V.; Widmark, P. O.; Serrano-Andres, L.; Lindh, R.; Roos, B. O. *Int. J. Quantum Chem.* **2004**, *100*, 626−635.

(39) Chilton, N. F.; Collison, D.; McInnes, E. J. L.; Winpenny, R. E. P.; Soncini, A. *Nat. Commun.* **2013**, *4*, 2551.

(40) McPhillips, T. M.; McPhillips, S. E.; Chiu, H. J.; Cohen, A. E.; Deacon, A. M.; Ellis, P. J.; Garman, E.; Gonzalez, A.; Sauter, N. K.; Phizackerley, R. P.; Soltis, S. M.; Kuhn, P. *J. Synchrotron Radiat.* **2002**, *9*, 401−406.

(41) Kabsch, W. *J. Appl. Crystallogr.* **1993**, *26*, 795−800.

(42) Sheldrick, G. M. *Acta Crystallogr., Sect. A* **2008**, *64*, 112−122.

(43) Barbour, L. J. *J. Supramol. Chem.* **2001**, *1*, 189−191.